Paramagnetically aligned spin density in the metallic phase of V_2O_3: evidence for orbital exchange correlation

1998 J. Phys.: Condens. Matter 10 9581

(http://iopscience.iop.org/0953-8984/10/42/022)

J. Phys.: Condens. Matter **10** (1998) 9581–9589. Printed in the UK PII: S0953-8984(98)96093-3

Paramagnetically aligned spin density in the metallic phase of V_2O_3: evidence for orbital exchange correlation

P J Brown†‡, M M R Costa§ and K R A Ziebeck‡

† Institut Laue Langevin, BP156 38042 Grenoble, France
‡ Department of Physics, Loughborough University, Leicestershire LE11 3TU, UK
§ Departamento de Fizica, Universidade de Coimbra, 3000 Coimbra, Portugal

Received 20 July 1998

Abstract. The spatial distribution of the magnetization induced in V_2O_3 at 180 K by a field of 4.6 T has been determined using polarized neutron diffraction. At this temperature, which is just above that of the metal–insulator transition, V_2O_3 is in the metallic phase which has the rhombohedral corundum structure. The susceptibility, which increases abruptly on raising the temperature through the transition at $\simeq$165 K, is $\simeq 12 \times 10^{-6}$ emu g^{-1} at 180 K and the moment aligned by 4.6 T at 180 K is 0.0082 μ_B/V. The magnetic structure factors were determined from the polarization dependence of the intensities of the Bragg reflections. The results show that the moment on the V atoms is almost entirely due to electrons in the doubly degenerate orbitals which are supposed to give rise to orbital ordering. There is also a significant negative moment amounting to some 6% of the total, associated with the oxygen sites which can only be due to exchange polarization.

1. Introduction

Materials exhibiting metal–insulator (Mott) transitions have been extensively studied ever since Mott suggested the possibility of this many-body phenomenon [1]. The materials which have received most attention are the Vanadium oxides, in particular vanadium sesquioxide V_2O_3 and its alloys with Cr [2, 3, 4]. Mott [5] has said of V_2O_3 'there are almost as many theories for this material as there are theorists who have discussed it'. V_2O_3 is an insulating antiferromagnet at low temperatures. Near 165 K the stoichiometric compound undergoes a sharp phase transition to a metallic state without long-range magnetic order and at around 550 K the material gradually transforms back to an insulating phase. Doping with chromium raises the temperature of the lower transition and lowers that of the higher, until at a chromium content of some 1.5% the metallic phase is completely suppressed [6]. Surplus oxygen, on the other hand, decreases the stability range of the low-temperature insulating phase and $V_{1.97}O_3$ remains metallic down to the lowest temperatures [7].

In stoichiometric V_2O_3 the metal to insulator transition which occurs on cooling below $\simeq$165 K is accompanied by the appearance of long-range antiferromagnetic order [8] and a structural distortion of the trigonal (corundum) structure to a low-temperature monoclinic form resulting in a discontinuous expansion of nearest-neighbour V–V distances [9]. The magnetic susceptibility is anomalously high in the metallic phase and drops abruptly by a factor of nearly 2 at the transition [10]. NMR and susceptibility measurements have been combined to separate the contributions to the susceptibility in the metallic phase into

0953-8984/98/429581+09$19.50

temperature-independent diamagnetic (dia) and Van Vleck (VV) parts and a temperature-dependent 3d part obeying a Curie–Weiss law

$$\chi(T) = \chi_d(T) + \chi_{VV} + \chi_{dia} \qquad \text{and} \qquad \chi_d(t) = C/(T+\theta)$$

with $C = 0.657$ emu mol^{-1} K^{-1} and $\theta = -600$ K giving $\mu_{eff} = 2.37\ \mu_B$ per V [11]. Heat capacity measurements show a large electronic contribution (130×10^{-4} cal K^{-2} mol^{-1}) and comparison between effective masses calculated from heat capacity, magnetic susceptibility and optical properties suggests that the mass enhancement arises mainly from spin fluctuations [7]

In spite of considerable experimental and theoretical effort the precise mechanisms giving rise to the phase transitions in V_2O_3 remain unclear [12]. Broken symmetries invoking magnetic and excitonic order parameters, electron–phonon coupling, Peierls transition, charge density waves, strong correlation effects leading to an almost degenerate Fermi liquid, and various combinations of these possibilities have been invoked to account for the observed physical properties. Recently there has been renewed interest in these materials aroused by the discovery of high-T_c superconductivity in copper-based transition metal oxides. The vanadium oxides show similar properties with metallic states close in energy to insulating antiferromagnetic states although superconductivity has not been found. Rice [13] has refocused attention on the role of orbital–spin coupling in the vanadium and titanium oxides, an effect which was introduced and developed in detail by Castellani, Natoli and Ranniger [14, 15, 16]. The orbital–spin coupling is a nonrelativistic effect arising when the the superexchange interactions involving partly occupied degenerate orbitals lead to strong coupling between orbital and spin structures. Support is lent to this model by a recent neutron scattering study of magnetic correlations in both the metallic and insulating phases of pure and doped V_2O_3 [17]. It was shown that the transition to the insulating antiferromagnetic phase from either paramagnetic phase is accompanied by an abrupt change in the dynamic short-range order and that the metallic phase is characterized by incommensurate spin correlations. On the basis of these results it was conjectured that the transition to the antiferromagnetic insulator is associated with orbital ordering and orbital rather than spin fluctuations characterize the paramagnetic state.

The orbital ordering model [14] presupposes that the unpaired electrons in V_2O_3 occupy a particular set of 3d orbitals. This implies that the electron density associated with these orbitals will have a characteristic spatial distribution. Since it is these same electrons which give rise to the paramagnetic susceptibility in the metallic phase, their spatial distribution is accessible through that of the magnetization aligned by a magnetic field. This paper reports a determination of this magnetization distribution using polarized neutron flipping ratio measurements to determine the scattering due to the magnetic moment aligned by a field of 4.6 T at 180 K.

2. Experimental details

The samples used in the present work were single crystals obtained from Cristal-Tec, Grenoble; they were of irregular form and had dimensions $\simeq 4 \times 3 \times 3$ mm. Two different but similarly sized crystals were used.

2.1. Magnetization

The susceptibility of one of the crystals was measured at 180 K using a squid magnetometer (Quantum Design). The magnetization was found to be a linear function of field up to the

maximum applied (5.5 T). The magnetization induced at 180 K by a field of 4.6 T was 0.6124 emu g^{-1} which corresponds to a moment of 0.00822 μ_B per vanadium atom.

2.2. Unpolarized neutrons

In order to check the crystal structure, and to determine to what degree extinction was present in the crystals, sets of integrated intensities were measured for both crystals at wavelengths of 0.84 and 0.54 Å. The measurements were made at 180 K using the double stage Displex refrigerator on the D9 single crystal diffractometer at ILL. The measurements extended to $\sin\theta/\lambda$ = 0.86 $Å^{-1}$ for $\lambda = 0.84$ Å and to $\sin\theta/\lambda$ = 1.0 $Å^{-1}$ for $\lambda = 0.54$ Å. Experimental nuclear structure factors were calculated from the integrated intensities and were used as data in least-squares refinements. The parameters varied in the refinement were: the V z and O x coordinates, the isotropic temperature factor (ITF) for O, the scattering length b_V of V, a single extinction parameter η to model the mosaic spread, and a scale factor for each wavelength. The V scattering length was included because of its small value which makes it particularly sensitive to any impurity on the V sites. The V ITF was fixed at 0.3 $Å^{-2}$ for the same reason. Separate refinements were carried out for each crystal. The results are given in table 1. The parameters obtained for the two crystals are in good agreement except for a small difference in the x_O value. The value 0.3126 obtained for crystal A, which gave the better refinement, was used in further processing.

Table 1. Crystallographic data and results of structure refinement for V_2O_3.

Space group:		$R\bar{3}c$	Hexagonal axes				
Unit cell:		$a = 4.952$ Å	$c = 14.002$ Å				
Atomic positions:		12 V in 12 (c)	0 0 z_V				
		18 O in 18 (e)	x_O 0 $\frac{1}{4}$				
Crystal	z_V	b_V (fm)	x_O	B_O ($Å^{-2}$)	η†	R (%)	N°_{obs}‡
A	0.3455(3)	−0.471(11)	0.31255(5)	0.413(7)	0.137(12)	4.3	543
B	0.3456(5)	−0.471(17)	0.31351(14)	0.482(12)	0.095(11)	7.2	463

† The mosaic spread parameter of the extinction model in units of 10^{-4} rad^{-1}.
‡ The number of independent reflections included in the refinement.

2.3. Polarized neutron measurements

Polarized neutron flipping ratios were measured on the D3 polarized neutron diffractometer at ILL. The two crystals which had been measured with unpolarized neutrons were mounted, one with a $[1\bar{1}.0]$ axis and the other with a [01.0] axis vertical. For the measurements they were fixed in the variable temperature chamber at the centre of a split pair superconducting magnet giving a vertical field of 4.6 T. The sample temperature was maintained at 180 K. For both crystals measurements were made of all the Bragg reflections on the zero and first layers with $\sin\theta/\lambda < 0.5$ $Å^{-1}$ whose nuclear structure factors (per hexagonal cell) were greater than 0.4×10^{-13} cm. The neutron wavelength was 0.843 Å. Reflections for which the standard deviation in the magnetic structure factor after measuring the flipping ratio for 90 min was greater than 5×10^{-16} cm were not pursued further. Cyclic measurement of the remainder of the reflections was continued for all the time available, reflections being removed from the cycle when the estimated standard deviation of their magnetic structure factor dropped below 10^{-16} cm.

The magnetic structure factors were calculated from the measured flipping ratios using the structure parameters obtained from the unpolarized measurements (see the previous section). The procedure used takes into account incomplete polarization of the incident beam, the inclination of the scattering vector to the horizontal plane and extinction using the single parameter model fitted to the integrated intensity measurements [18]. The maximum extinction correction was 1.44 for the 006 reflection. Each magnetic structure factor was obtained from the average of several measurements of at least two equivalent reflections. The final list of observed magnetic structure factors is given in table 2; they contain a small diamagnetic contribution which has been estimated [19] and is also given in table 2.

Table 2. Observed and calculated magnetic structure factors† for V_2O_3 at 180 K in 4.6 T $\perp$ $\boldsymbol{c}$.

				Crystal B		Crystal A			Mean F_{dia}		Models	
h	k	ℓ	$\sin\theta/\lambda$ (Å^{-1})	F_{obs}	ΔF_{obs}	F_{obs}	ΔF_{obs}	Diamagnetism F_{dia}	F_{obs}	ΔF_{obs}	F_{calc}‡	F_{calc}§
1	0	2	0.1367	−25.6	2.1	−26.6	1.6	0.1	−26.3	1.3	−27.1	−24.9
1	0	$\bar{4}$	0.1844	−45.0	1.5	−44.6	1.9	0.1	−44.9	1.2	−46.1	−46.6
1	1	0	0.2019	54.1	4.5	65.7	4.3	−0.0	60.1	5.8	58.0	53.8
0	0	6	0.2143	65.5	2.0	73.7	2.1	0.2	69.3	4.1	49.1	58.7
1	1	3	0.2286	−0.2	2.4	−5.0	4.1	−0.3	−1.2	2.1	0.0	−4.6
2	0	$\bar{2}$	0.2439			−17.6	1.6	0.0	−17.6	1.6	−17.1	−16.0
2	0	4	0.2734			−25.9	2.9	0.2	−26.1	2.9	−29.5	−28.9
1	1	6	0.2944			35.1	5.8	−0.3	35.4	5.8	31.7	34.6
1	0	8	0.3085			1.2	4.9	−0.0	1.2	4.9	2.8	3.6
2	1	$\bar{1}$	0.3105			−6.1	3.1	−0.1	−6.1	3.1	0.0	−1.0
2	1	2	0.3166	−17.1	5.8	−6.4	3.2	0.0	−9.0	4.5	−11.1	−9.9
2	1	$\bar{4}$	0.3399	−6.7	6.0			0.1	−6.8	6.0	−19.4	−18.7
3	0	0	0.3498			17.5	4.8	−0.4	17.9	4.8	24.6	18.6
2	1	5	0.3564	6.1	9.2	−10.0	9.8	0.1	−1.5	8.1	0.0	0.9
2	0	$\bar{8}$	0.3688			7.8	7.8	0.0	7.8	7.8	1.9	2.7
1	1	9	0.3796	−3.6	2.4	−11.0	9.1	0.2	−4.3	2.3	0.0	−0.7
2	1	$\bar{7}$	0.3970	0.4	7.6	−9.3	8.9	0.1	−3.7	5.8	0.0	−3.9
2	2	0	0.4039	16.5	3.3			−0.0	16.6	3.3	16.4	13.0
3	0	6	0.4102			14.8	5.1	0.1	14.7	5.1	14.0	16.8
3	0	$\bar{6}$	0.4102			19.2	3.8	0.1	19.1	3.8	14.0	16.8
2	2	3	0.4178	−6.7	2.7			0.2	−7.0	2.7	0.0	−3.9
3	1	1	0.4219			−5.0	4.9	−0.0	−4.9	4.9	0.0	0.5
2	0	,10	0.4265			−19.2	5.3	0.1	−19.3	5.3	−13.2	−22.2
0	0	,12	0.4285	15.7	3.2	11.6	2.7	−0.4	13.7	2.0	8.2	15.1
3	1	4	0.4440			−12.6	4.0	0.1	−12.7	4.0	−8.7	−8.0
2	2	6	0.4572	12.1	3.0			−0.3	12.3	3.0	9.4	10.4
1	1	,12	0.4737	5.7	2.6			0.0	5.7	2.6	5.5	12.0

† All magnetic structure factors are given in units of 10^{-3} μ_B per hexagonal cell.
‡ Structure factors calculated for a spherical V^{3+} spin only moment of 7.8×10^{-3} μ_B.
§ Structure factors calculated for 7.31×10^{-3} unpaired electrons in V 3d e_{g1} orbitals and 0.4×10^{-3} electrons of opposite spin in O 2s orbitals. The combination $\langle j_0\rangle + 0.24\langle j_2\rangle$ was used for the dipole term in the V form factor.

3. Analysis of the results

According to the susceptibility measurements the magnetization induced in our crystals at 180 K by the applied field of 4.6 T is 8.22×10^{-3} μ_B per V atom of which -0.08 is due to diamagnetism [11]. On the other hand the best fit between the observed magnetic structure factors given in table 2 and the scattering due to the sum of spherically symmetric

V^{3+} ions at the V sites is obtained with a V moment of only $7.8(2) \times 10^{-3}\ \mu_B$, which suggests that some of the magnetization is delocalized. The experimental data may also be represented pictorially as points on a form factor as in figure 1. In this diagram the value plotted at each of the experimental points is $(M_{obs} - M_{dia})/\cos(2\pi \ell z_V)$. The cosine term is the geometric structure factor of the V atoms. The full curve given for comparison is the 3d spherical form factor for the V^{3+} ion normalized to $8.2 \times 10^{-3}\ \mu_B$. The reflections with odd ℓ are special and would have no magnetic contribution at all if all the magnetization were spherically distributed around the V ions, they are shown as open circles. It can be seen that although most of the points lie near to the plotted curve, there are some significant deviations which justify the development of a more sophisticated model.

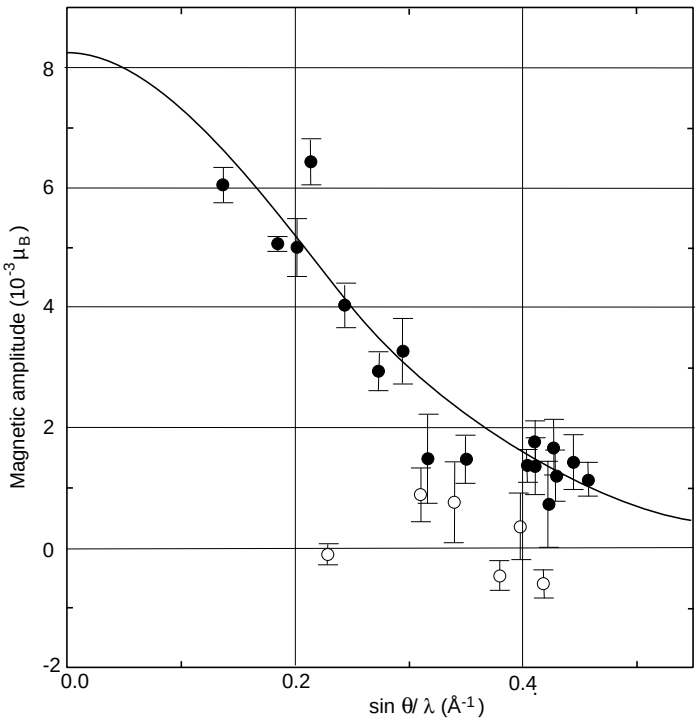

Figure 1. The magnetic amplitude per V^{3+} ion induced in V_2O_3 by a field of 4.6 T at 180 K. The points denoted by ● are for reflections with ℓ even and those marked ○ are for ℓ odd. The full curve is the V^{3+} $\langle j_0 \rangle$ 3d form factor normalized to $8.2 \times 10^{-3}\ \mu_B$.

3.1. Maximum entropy reconstruction

It has been shown that when only sparse and noisy data are available reconstruction of an image from a set of observations using a maximum entropy algorithm is more reliable than direct fourier transformation [20]. Papoular and Gillon [21] have shown how the method can be used to reconstruct the magnetization distribution from magnetic structure factors measured using the polarized neutron technique. In the present case the maximum entropy algorithm [22] has been used to reconstruct the density corresponding to the differences between the observed magnetic structure factors and those calculated for V^{3+} spherical 3d moments of $7.8 \times 10^{-3}\ \mu_B$ centred at each V site; this is the magnetic equivalent of the

maximum entropy deformation density [23]. This difference density was calculated for a single rhombohedral cell over a mesh of $32 \times 32 \times 32$ points. The calculated values were then interpolated in order to obtain sections in the principal symmetry directions. The section parallel to (01.0) passing through the origin is shown in figure 2.

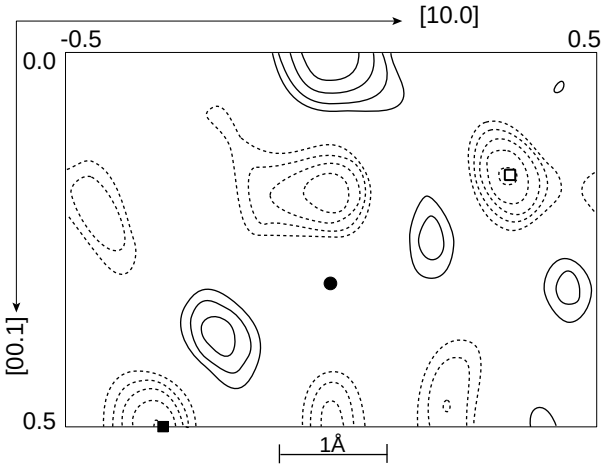

Figure 2. The section, parallel to (01.0) passing through the origin, of the maximum entropy reconstruction of the difference between the observed magnetization distribution and that due to spherically symmetric V^{3+} spin. The ● marks the position of the V^{3+} ion, the ■ that of the O^{2-} ion in the plane of the section and the □ that of the O^{2-} which is 0.1 Å below it. The contours are logarithmically spaced with a factor of two between successive levels. The highest contour is at 0.33×10^{-3} μ_B Å^{-3}.

The most significant features of the difference density are:

(i) negative density around the O sites,
(ii) areas of positive and negative density surrounding the V sites; the positive areas are located on the V–O bonds.

These observations suggest that a more realistic model of the magnetization distribution should include the possibility of a magnetic moment on the oxygen sites, and should allow a non-spherical moment distribution around the V sites.

3.2. Multipole fits to the density

The V site in V_2O_3 lies on the triad axis, but has no other symmetry. The real combinations of even multipole functions permitted by this symmetry up to order 4 are:

$$\begin{aligned} &Y(00) = Y_0^0 \qquad Y(20) = Y_2^0 \qquad Y(40) = Y_4^0 \\ &Y(43+) = (Y_4^{-3} + Y_4^3)/\sqrt{2} \qquad Y(43-) = \mathrm{i}(Y_4^3 - Y_4^{-3})/\sqrt{2}. \end{aligned} \tag{1}$$

The amplitudes of these functions, together with that of a $Y(00)$ 2s function, centred on the O sites, were allowed to vary in a multipole refinement using the observed magnetic structure factors as data. The results are shown in table 3; the only significant amplitudes are those of $Y(00)$, $Y(20)$, $Y(43-)$ for V and $Y(00)$ for O. In trigonal symmetry and taking

the triad axis as the z direction, the five orbital d functions split into a singly degenerate a_1 function and two sets of doubly degenerate e_g functions:

$$\begin{aligned} a_1 &= Y_2^0 \\ e_g(11) &= [\sqrt{2}(Y_2^{-2} + Y_2^2) + \mathrm{i}(Y_2^{-1} + Y_2^1)]/\sqrt{3} \\ e_g(12) &= [\sqrt{2}\mathrm{i}(Y_2^{-2} - Y_2^{+2}) - (Y_2^{-1} - Y_2^{+1})]/\sqrt{3} \\ e_g(21) &= [(Y_2^{-2} + Y_2^2) - \mathrm{i}\sqrt{2}(Y_2^{-1} + Y_2^{+1})]/\sqrt{3} \\ e_g(22) &= [\mathrm{i}(Y_2^{-2} - Y_2^2) + \sqrt{2}(Y_2^{-1} - Y_2^{+1})]/\sqrt{3} \end{aligned} \tag{2}$$

the corresponding densities are:

$$\begin{aligned} |a_1|^2 &= Y(00) + \tfrac{\sqrt{20}}{7}Y(20) + \tfrac{6}{7}Y(40) \\ \tfrac{1}{2}\left(|e_g(11)|^2 + |e_g(12)|^2\right) &= Y(00) - \tfrac{\sqrt{5}}{7}Y(20) - \tfrac{2}{21}Y(40) + \sqrt{\tfrac{20}{63}}Y(43-) \\ \tfrac{1}{2}\left(|e_g(21)|^2 + |e_g(22)|^2\right) &= Y(00) + \tfrac{1}{3}Y(40) - \sqrt{\tfrac{20}{63}}Y(43-). \end{aligned} \tag{3}$$

These results, taken in conjunction with the multipole fit, strongly suggest that the bulk of the V magnetization is associated with the $e_g(11)$ and $e_g(12)$ orbitals which are henceforward collectively designated e_{g1}. In light of these results some further refinements were carried out in which various constraints were imposed on the multipole parameters. The results of some of these refinements are summarized in table 3. The best fit to the data was obtained with a V 3d moment of 0.0072(3) μ_B, all in the e_{g1} orbitals, and an oxygen moment of $-0.0004(2)$ μ_B. The spherical part of the 3d moment was fitted in the dipole approximation [24] by $\langle j_0\rangle + c\langle j_2\rangle$ with $c = 0.24(14)$. This gives a total moment of 0.0067(4) μ_B/V, rather less than the 0.0082 μ_B obtained from the bulk magnetization, suggesting that some of the magnetic moment is delocalized and does not contribute to the Bragg scattering.

Table 3. Results of some multipole fits to the magnetization distribution in V_2O_3†.

		A		**B**		**C**		**D**	
Atom	Function	Free		μ fixed		μ free		**C** with V_{orb}	
	$Y(00)\langle j0\rangle$	7.6	0.2	7.9		7.5	0.2	7.2	0.3
	$Y(00)\langle j2\rangle$	0.0		0.0		0.0		1.7	1.0
V 3d	$Y(20)$	−1.2	0.8	−1.2	0.9	−2.4		−2.3	
	$Y(40)$	−0.3	2.2	−0.4	2.5	−0.7		−0.7	
	$Y(43+)$	0.2	2.6	0.4	2.8	0.0		0.0	
	$Y(43-)$	5.7	2.7	6.1	3.0	4.2		4.0	
O 2s	$Y(00)$	−0.4	0.3	−0.4	0.2	−0.4	0.2	−0.4	0.2
	χ^2 ‡	2.15		2.50		2.01		1.84	

† For each model the multipole parameters with their estimated standard deviations (esd) are given in units of 10^{-3} μ_B, where no esd is given the ratio of that parameter to one of the others was fixed by the model.

‡ $\chi^2 = \left[\sum_{observations}(F_{obs} - F_{calc})^2/(\Delta F_{obs})^2\right]/(n_{observations} - n_{parameters})$.

4. Discussion

The negative magnetic moment associated with the O^{2-} ions is quite unexpected, since in an aligned paramagnet any covalent interaction between the electrons contributing to the

magnetization and their oxygen neighbours would be expected to transfer moment from V^{3+} to $O^{2-}$and lead to positive density at the O sites. A negative ligand density in exchange coupled systems can arise from exchange polarization. This is due to differences between the covalent mixing parameters for the doubly occupied (mainly ligand) orbitals. The exchange interaction lowers the energies of the positive, relative to the negative, spin d-states; the d participation in the positive spin state is increased and the ligand contribution reduced, the opposite being true for the negative spin state. If the corresponding antibonding (mainly d) states are not fully occupied the result is a negative ligand moment. No appreciable exchange polarization should occur in an aligned paramagnetic metal unless there is significant exchange enhancement of the moment.

As indicated above a small improvement in the goodness of fit was obtained by allowing the V form factor to assume some orbital character. This may indicate that about 24% of the susceptibility is due to orbital moments. Alternatively, the apparent expansion of the form factor could arise from curtailment of the V density by negative overlap from the ligands. The relatively small orbital moment is somewhat at variance with the recent NMR study [25] in which it is concluded that nuclear relaxation at high temperatures is almost entirely due to orbital moments.

The anisotropy of the magnetization distribution around V is characteristic of the 3d orbitals of e_{g1} symmetry described in the previous section; the a_1 orbitals make an insignificant contribution. The recent band-structure calculation [26] finds that the partially filled bands at the Fermi surface involve all five a_1, e_{g1} and e_{g2} states. The densities of the e_{g1} and e_{g2} states at the Fermi surface are approximately equal and about three times greater than that of the a_1 states. It might therefore be expected that e_{g1} and e_{g2} states should contribute more or less equally to the susceptibility and hence to the aligned magnetization.

The orbital–spin coupling mechanism proposed in [14], which links the sign of the exchange interaction in antiferromagnetic V_2O_3 to the alignment of e_{g1} orbitals on near neighbour V atoms, provides a possible means of reconciling these conflicting results. There is evidence [17, 13] that strong correlations, which may be due to this process, persist in the paramagnetic metallic phase near to the metal–insulator transition. It should be emphasized that the states involved in the orbital–spin coupling have, to a first approximation, no orbital moment and so are consistent with the present observations. Orbital driven spin correlation would lead to exchange enhancement of the e_{g1} orbitals' contribution to the susceptibility, and hence to their dominance in the aligned magnetization. The same mechanism could provide the exchange energy required to polarize the doubly occupied ligand orbitals.

Acknowledgment

The authors would like to thank B Dennis for carrying out the magnetization measurements.

References

[1] Mott N F 1949 *Proc. Phys. Soc. (London)* **62** 416
[2] Föex M 1946 *C. R. Acad. Sci. Paris* **223** 1126
[3] Kosuge K 1967 *J. Phys. Chem. Solids* **28** 1613
[4] Feinleib J and Paul W 1967 *Phys. Rev.* **155** 841
[5] Mott N F 1973 *Contem. Phys.* **14** 401
[6] McWhan D B and Remeika J P 1970 *Phys. Rev.* B **2** 3734
[7] McWhan D B, Remeika J P, Malta J P, Okinaka H, Kosuge K and Kachi S 1972 *Phys. Rev.* B **7** 326
[8] Moon R M 1970 *Phys. Rev. Lett.* **25** 527
[9] Dernier P D and Marezio M 1970 *Phys. Rev.* B **2** 3371

[10] Carr P H and Foner S 1960 *J. Appl. Phys.* **31** 344S
[11] Jones E D 1965 *Phys. Rev.* **137** 978
[12] Kuwamoto H, Honig J M and Aeppli G 1980 *Phys. Rev.* B **22** 2626
[13] Rice T M 1995 *Spectroscopy of Mott Insulators and Correlated Metals* ed A Fujimori and Y Tokura (Berlin: Springer) p 221
[14] Castellani C, Natoli C R and Ranniger J 1978 *Phys. Rev.* B **18** 4945
[15] Castellani C, Natoli C R and Ranniger J 1978 *Phys. Rev.* B **18** 4967
[16] Castellani C, Natoli C R and Ranniger J 1978 *Phys. Rev.* B **18** 5001
[17] Bao W, Broholm C, Aeppli G, Dai P, Honig J M and Metcalf P 1997 *Phys. Rev. Lett.* **78** 507
[18] Delapalme A, Lander G H and Brown P J 1978 *J. Phys. C: Solid State Phys.* **11** 1441
[19] Stassis C 1970 *Phys. Rev. Lett.* **24** 1415
[20] Gull S F and Daniell G J 1978 *Nature* **272** 686
[21] Papoular R J and Gillon B 1990 *Europhys. Lett.* **13** 229
[22] Gull S F and Daniel G J 1989 *Quantified Maximum Entropy 'MEMSYS 3' Users Manual* Maximum Entropy Data Consultants Ltd, 33 North End, Meldreth Royston SG8 6NR, England
[23] Papoular R J, Vekhter Y and Coppens P 1996 *Acta Crystallogr*. A **52** 397
[24] Marshal W and Lovesey S W 1971 *Theory of Thermal Neutron Scattering* (Oxford: Oxford University Press) p 132
[25] Takigawa M, Ahrens E T and Ueda Y 1966 *Phys. Rev. Lett.* **76** 283
[26] Mattheiss L F 1994 *J. Phys.: Condens. Matter* **6** 6477